PAPER

Large angle beam steering using a slanted holographic polymer dispersed liquid crystal grating

IOP Publishing Journal of Physics D: Applied Physics
J. Phys. D: Appl. Phys. **51** (2018) 385103 (6pp) https://doi.org/10.1088/1361-6463/aad71b

Large angle beam steering using a slanted holographic polymer dispersed liquid crystal grating

Minghuan Liu[1,2], Zhihui Diao[1], Li Xuan[1], Zenghui Peng[1], Lishuang Yao[1], Qidong Wang[1], Zhaoliang Cao[1] and Yonggang Liu[1,3]

[1] State Key Laboratory of Applied Optics, Changchun Institute of Optics, Fine Mechanics and Physics, Chinese Academy of Sciences, Changchun 130033, People's Republic of China
[2] University of Chinese Academy of Sciences, Beijing 100049, People's Republic of China

E-mail: liuyonggang@ciomp.ac.cn

Received 6 March 2018, revised 24 July 2018
Accepted for publication 31 July 2018
Published 17 August 2018

Abstract

This paper reports 65° beam steering using a slanted holographic polymer dispersed liquid crystal (HPDLC) grating with the slanted angle at 16.6°. The HPDLC grating was fabricated using a convenient one-step holographic technique. The SEM image confirmed the slanted grating configuration. The grating showed anisotropic diffraction characterizations. The diffraction efficiency for the *p*-polarized light was as high as 80%. The Bragg angle deviation diffraction and the transmittance properties of the slanted HPDLC grating were investigated. The slanted HPDLC grating can be switched with an external electric field. The results in this work provide an optional method to fabricate a slanted grating configuration. The slanted HPDLC grating can be used in the field where polarized beam steering is required.

Keywords: holographic polymer dispersed liquid crystal, slanted grating, beam steering

(Some figures may appear in colour only in the online journal)

1. Introduction

Holographic polymer dispersed liquid crystals (HPDLCs) attract significant scientific curiosity and have been intensively researched recently [1, 2]. HPDLCs possess a Bragg volume grating structure, which are created by a polymerization-induced phase separation process using coherent multi-beams [3–5]. The input light is strongly diffracted when the incident angle matches the Bragg angle. The diffraction efficiency can be as high as 100% theoretically. The special characterization of HPDLCs is that the diffraction can be switched using external field because of the LC in the HPDLCs. HPDLCs are novel multi-function holographic optical elements (HOEs), which show promising prospects in the field of spatial light modulation [6–9].

Slanted gratings can be used as couplers to realize beam steering [10]. The reflection mode HPDLCs are designed to achieve the reflective display [11, 12]. Slanted reflection mode HPDLCs are fabricated to expand the viewing angle [13] and the total-internal-reflection mode HPDLCs is also achieved to guide the diffraction light to the sample edge [14]. Light manipulation using slanted grating has been implemented in holographic gelatin emulsions. One example demonstrated a complete 'U turn' of the incident light using a double slated reflection grating structure, however, the efficiency was no more than 10%, which restricts real applications [15]. Transmittance mode volume slanted gratings are better candidates to obtain higher diffraction efficiency because the diffraction efficiency can achieve 100% theoretically. HPDLCs have the capacity to switch the efficiency of such devices. Transmittance mode slanted gratings are desired to achieve the beam steering in axis so as to reduce the size of the optical setup. Thus, switching capability, large slant angle and high efficiency are desired for practical applications in beam steering. Sun *et al* pioneered the work to investigate slanted HPDLC gratings. They fabricated a 2.5° slanted HPDLC grating with a grating period of 286 nm, which had

[3] Author to whom any correspondence should be addressed.

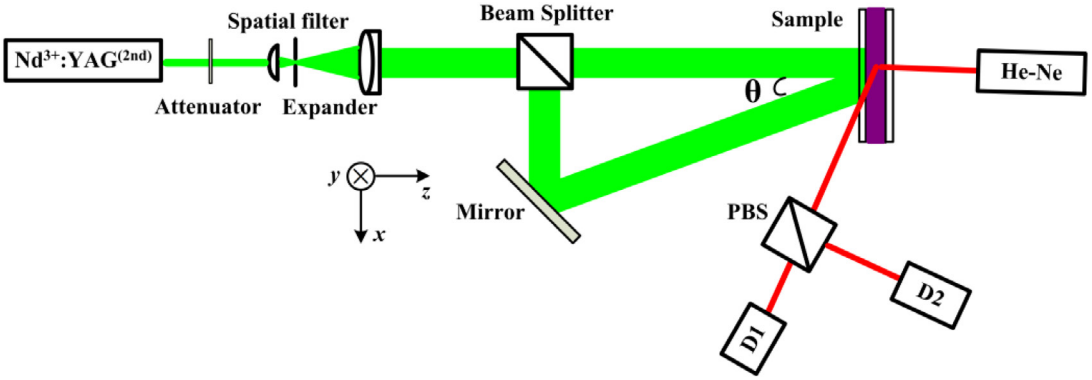

Figure 1. Schematic illustration of slanted HPDLC fabrication and characterization.

a diffraction efficiency up to 53% [16]. Thermal control of the 11° slanted HPDLC as a coupler with a grating period of 1 μm has also been reported, where 15% of the solar radiation was switched between the transmittance and diffraction states as a function of temperature at 30 °C. The diffraction efficiency was about 60% [17]. The dimensional changes in 10° slanted holographic gratings were investigated so as to obtain the formation dynamics. The results indicate that the shrinkage in HPLDC is so small that the angle deviation does not affect the maximum of diffraction efficiency significantly [18]. The holographic waveguide is achieved using a transmittance mode slanted HPDLC with the diffraction efficiency up to 42%. The coupling effect is better when a higher slanted HPDLC is used [19].

The two-beam interference setup is a simple configuration to fabricate slanted and unslanted HPDLC gratings [20], and is commonly used to make slanted volume gratings where both beams' angles of incidence are low enough to avoid the use of coupling prisms [21]. Both high diffraction efficiency and a high slant angle are desired when a slanted HPDLC is used in fields such as beam steering and couplers. Thus, the fabrication of a high efficiency slanted HPDLC grating with a large slanted angle is of significant urgency. Such work can make insights into the working mechanism and obtain comprehensive understanding for slanted transmittance mode HPDLC. In a previous work, we reported an unslanted transmittance mode HPDLC using a commercial five functionality acrylate monomer dipentaerythritol hydroxyl pentaacrylate (DPHPA). A cross section view instead of the conventional top view is used to characterize the morphology. The morphology imaged by scanning electron microscope (SEM) indicated the superior volume grating structure [22].

In this work, we demonstrated a 65° angle beam steering using a 16.6° slanted HPDLC by a one-step holographic technique. Non-symmetry exposure setup without refractive index matching prisms was constructed. The diffraction evolution characterizations were investigated by a 632.8 nm He–Ne laser, which entered the sample at the Bragg angle. The slanted HPDLC was confirmed by a SEM image. The Bragg angle deviation, the transmittance spectrum and the electric field switching properties of the slanted HPDLC grating were studied.

2. Experiment

2.1. Materials

A pre-polymer mixture was made up so as to fabricate slanted transmittance mode HPDLC grating [23]. The nematic liquid crystal TEB-30A (29.4 wt.%) was provided by Silichem. The ordinary and extraordinary effective index of the liquid crystal used in this work were 1.522 and 1.692, respectively. The monomer was a commercially available five functionality acrylate monomer DPHPA (58.8 wt.%). The crosslinking agent N-vinylpyrrolidone (NVP, 9.8 wt.%), photo-initiator Rose Bengal (RB, 0.5 wt.%) and co-initiator N-phenylglycine (NPG, 1.5 wt.%) were also added into the mixture. The DPHPA, NVP, RB and NPG were purchased from Aldrich without further purification. The mixture was stirred to ensure an isotropic and homogeneous material system for 48 h in a dark room. The refractive index of the mixture is 1.537 @589.0 nm using an Abbe refractometer (2 WA, Kernco) after single beam exposure. The mixture was injected into a clean sample glass cell via calibration force in a darkroom. The glass plates possessed an indium tin oxide (ITO) layer. As a result, the electric field can be applied to the sample. The thickness of the glass cells was controlled at 9 μm using spacers.

2.2. Slanted HPDLC fabrication and characterization

The schematic experimental setup for slanted HPDLC fabrication and characterization is depicted in figure 1. A continuous *s*-polarized 532 nm laser, which was delivered from a neodymium-doped yttrium aluminum garnet (Nd^{3+}:YAG, second-harmonic generation [24, 25], New Industries Optoelectronics), was used to illuminate the sample. The input laser beams were expanded, spatially filtered and collimated into a uniform plane wave. Then, the beams were split into object and reference beams so as to construct the two-beam interference geometry. The interference pattern between the object and reference beams was recorded by the sample, which constructed the slanted HPDLC gratings. The grating period Λ was determined by the intersection angle between the object and the reference beams. The grating period Λ is expressed as [16]

$$\Lambda = \frac{\lambda_{\text{rec}}}{2n_G \sin[\arcsin(\sin\theta/n_G)/2]}, \quad (1)$$

where λ_{rec} is the recording laser wavelength in vacuum, n_G is the refractive index of the fabricating grating and θ is the intersection angle between the object and reference beams in the air. The slanted angle is expressed as

$$\theta_s = \arcsin[\sin(\frac{\theta}{2})/n_G], \quad (2)$$

A continuous 632.8 nm laser delivered from a He–Ne laser was used to investigate the time evolution of diffraction efficiency in real time, as shown in figure 1. The 632.8 nm laser has no influences on the grating evolution. The 632.8 nm laser entered the sample at the Bragg angle. A polarized beam splitter (PBS) was used to divide the diffraction beams into *s*-polarized and *p*-polarized parts. The intensities of the *s*-polarized and *p*-polarized diffraction beams were detected by photodiodes. The evolution of the diffraction efficiency is defined as

$$\eta_{p(s)} = \frac{I_{difp(s)}}{I_{incp(s)}}, \quad (3)$$

where I_{dif} is the diffraction intensity and I_{inc} is the incident intensity of the *p*-polarization and *s*-polarization beams. The scatterings loss cannot be tested because of the geometry of the setup used.

2.3. Grating morphology and transmittance spectrum characterization

The samples were disassembled so as to obtain slanted grating films. The slanted grating films were dissolved in ethanol for 24 h to remove the LCs. The slanted grating films were evaporated with Au atoms to enhance the conductivity before conducting the SEM characterization. The cross view was chosen to confirm the slanted Bragg volume grating geometry.

The transmittance spectra of the samples were performed by UV-3101PC ultraviolet–visible (UV–VIS) spectrometer (SHIMADZU). The sampling wavelength ranged from 380 to 780 nm so as to cover the whole visible band range.

2.4. Electrical field switching and Bragg angle deviation

The electric field was applied to the sample using a variable transformer as for electric field switching, as shown in figure 2. The sample was stabilized using a sample holder, which possessed a rotation precision at 1′. A 632.8 nm He–Ne laser entered the sample at the Bragg angle θ_B. Photodiodes D_1 and D_2 were used to detect the transmittance and diffraction intensity. A polarizer was used to polarize the incident light.

The variable transformer was removed so as to investigate the Bragg angle deviation. The Bragg angle deviation diffraction intensity was detected by rotating the sample holder. Since the incident light deviated from the Bragg angle, the direction of the diffraction light changed. Thus, the location of the photodiode D_2 should be replaced so as to match the diffraction light.

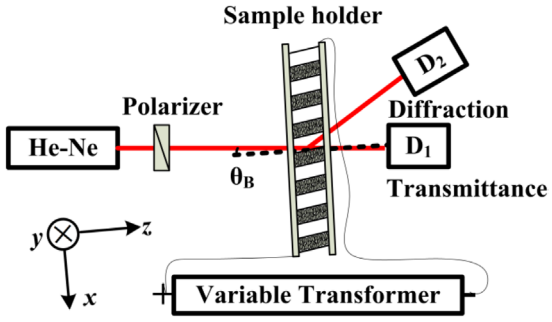

Figure 2. Schematic illustration of electric field switching and Bragg angle deviation.

3. Results and discussion

3.1. Grating evolution and LC orientation

According to the anisotropic coupled-wave theory [26], the diffraction efficiency of the HPDLC grating is determined as

$$\eta_p = \sin^2[\frac{\pi d(\cos^2\theta_B\varepsilon_{1x} - \sin^2\theta_B\varepsilon_{1z})}{2\lambda_p n_{ave}\cos\theta_B}] \quad (4)$$

and

$$\eta_s = \sin^2(\frac{\pi d\varepsilon_{1y}}{2\lambda_p n_{ave}\cos\theta_B}) \quad (5)$$

where ε_{1i} $(i = x, y, z)$ is the diagonal components of the relative permittivity modulation tensor, d is the grating thickness, θ_B is the Bragg angle in the grating, λ_p is the probe wavelength in vacuum, and n_{ave} is the average refractive index of the grating.

The time evolution property of the diffraction efficiency during the slanted HPDLC formation is shown in figure 3. The grating period is 650 nm. The diffraction efficiency possessed an oxygen depletion period for both *p*- and *s*-polarized probe lights [3]. After which, the polymerization-induced phase separation began. The diffraction efficiency for the *p*-polarized probe light increased with time and peaked within several seconds. The diffraction efficiency for *s*-polarized probe light peaked within several seconds and decreased approximately to zero with time. The diffraction efficiency values were 80.0 and 4.0% for the *p*- and *s*-polarized probe light, respectively. The η_p/η_s ratio is as high as 20. The distinct diffraction properties indicate that the slanted HPDLC grating possesses anisotropic properties during the grating formation. According to the anisotropic coupled-wave theory for a volume grating [26], the orientation of the LC in the slanted HPDLC grating is along the grating vector in the *x*-*z* plane, as shown in figure 2.

The dependence of diffraction efficiency values to illumination intensity is shown in figure 4. The diffraction efficiency reached maximum using the same time for each of the illumination intensities. The exposure time was 3 min for all of the samples. The maximum diffraction efficiency values were 45, 68, 80, 60 and 25% with illumination intensities at 2.6, 2.7,

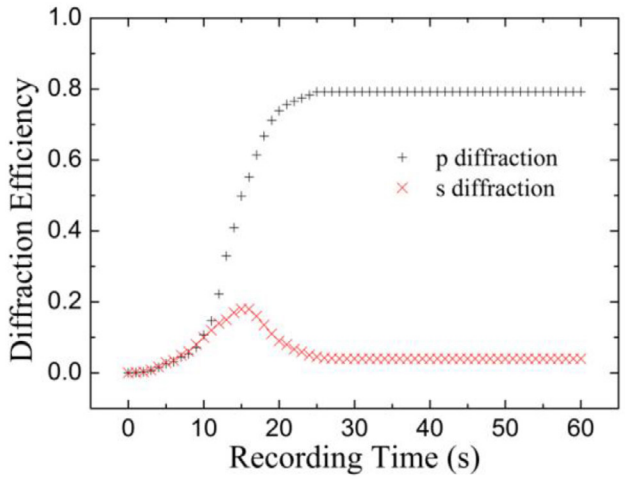

Figure 3. Time evolution characterizations of diffraction efficiency for the slanted HPDLC grating formation.

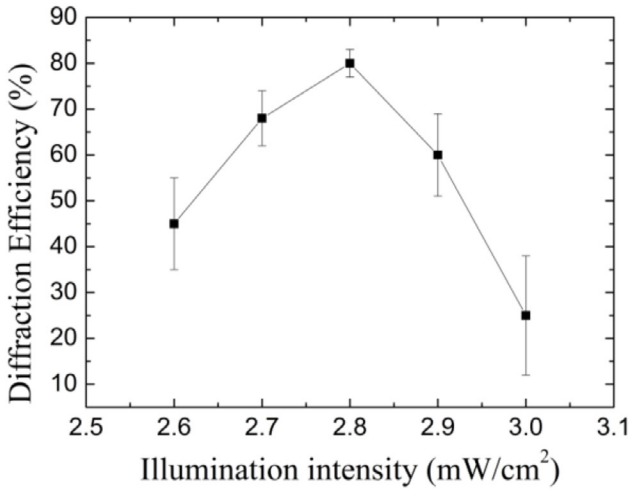

Figure 4. Diffraction efficiency as a function of illumination intensity.

2.8, 2.9 and 3.0 mW cm^{-2}, respectively. The error was 20, 12, 6, 18 and 26% with illumination intensities at 2.6, 2.7, 2.8, 2.9 and 3.0 mW cm^{-2}, respectively. The optimum illumination intensity was 2.8 mW cm^{-2}. The maximum diffraction efficiency values decreased with the deviation to the optimum illumination intensity [27].

3.2. Slanted grating morphology and beam steering

The morphology of a slanted HPDLC grating imaged by SEM is shown in figure 5. It confirms that the grating is truly slanted. The uniform HPDLC grating is a period structure with alternating LC and polymer layers. The couplers can be achieved using the slanted HPDLC grating by adjusting the grating period and the slanted angle [28]. The diffraction of a Bragg volume grating can be expressed as [23]

$$m\lambda_p = 2n_{ave}\Lambda \sin\theta_B, \tag{6}$$

where $m = 1$ denotes the diffraction order, $\lambda_p = 632.8$ nm is the probe wavelength, n_{eff} is the average refractive index

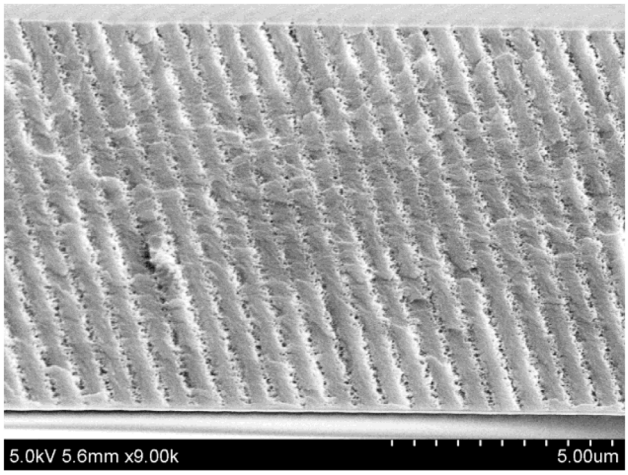

Figure 5. SEM image of the slanted HPDLC grating.

of the Bragg volume grating and θ_B is the Bragg diffraction angle. Substituting the parameters into equation (4), the Bragg diffraction angle θ_B is 18.48° in the slanted HPDLC grating. The incident angle is 1.84° and 35.12° for the incident and diffraction light, respectively, considering the 16.64° slanted angle of the slanted HPDLC grating. According to Snell's law, the incident angle is 2.83° and 62.0° in the air, respectively. The experimental values are 2.85° and 62.0°, which are in good agreement with the theoretical calculations. The beam steering experiment using the slanted HPDLC grating is shown in figure 6(a). Figure 6(b) shows the schematic illustration of the beam steering. The incident laser beams with *p*-polarization was effectively diffracted when the incident angle matched the Bragg angle. The beam steering angle is as high as 65°. The efficiency is as high as 95% when only taking transmittance and steering beams into consideration [28]. The 65° beam steering angle is the largest angle we have obtained with our present system. We have achieved good 48° and 37° beam steering with the intersection angle of the exposure laser beams at 40° and 30°, respectively. An 80° beam steering with the intersection angle of the exposure laser beams at 60° was achieved, however, the diffraction efficiency was no more than 15%. The 16.6° slanted angle slanted HPDLC with diffraction efficiency up to 80% is better than the reported results in [16–19].

3.3. Bragg angle deviation and gap

According to the coupled-wave theory [29], the diffraction efficiency of a slanted transmittance grating with the probe light deviating from the Bragg angle is expressed as follows:

$$\eta = \sin^2(\nu^2 + \xi^2)^{1/2}/(1 + \xi^2/\nu^2). \tag{7}$$

The parameters of ν and ξ in equation (5) are determined by

$$\nu = \frac{\pi\Delta n d}{\lambda_p(c_r c_s)^{1/2}} \tag{8}$$

and

$$\xi = \Delta\theta G_0 d \sin(\varphi - \theta_0)/(2c_s), \tag{9}$$

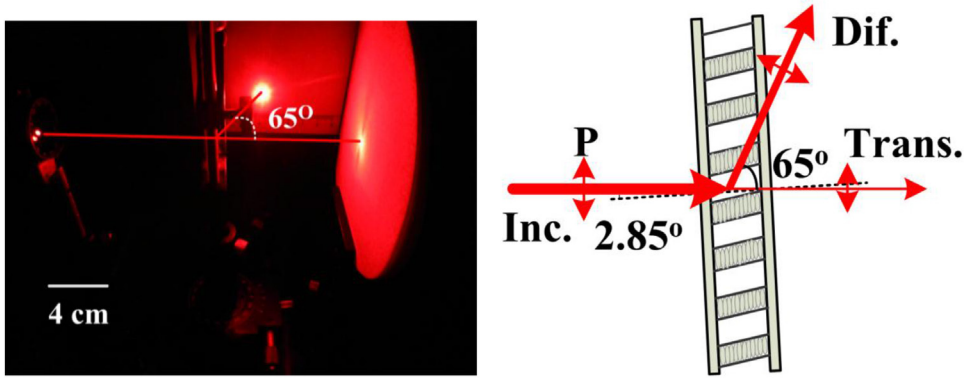

(a) (b)

Figure 6. Beam steering using the slanted HPDLC grating. (a) Actual experiment and (b) schematic illustration.

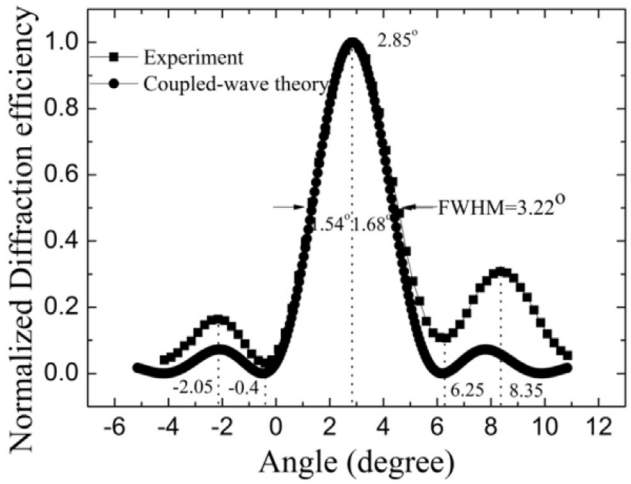

Figure 7. Normalized diffraction efficiency as a function of incident angle deviation.

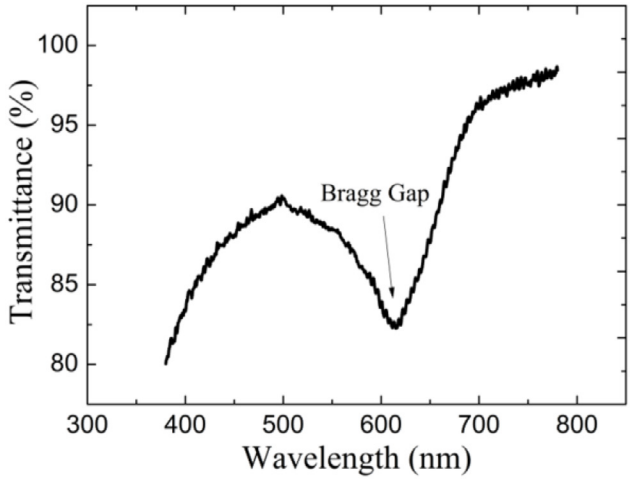

Figure 8. Transmittance spectrum as a function of wavelength for the slanted HPDLC.

where Δn is the refractive index modulation, d is the thickness of the grating, λ_p is the probe wavelength in vacuum, $\Delta\theta$ is the deviation angle, φ is the complementary angle of the grating slanted angle in the grating, θ_0 is the Bragg angle in the grating, $G_0 = 2\pi/\Lambda$ is the grating reciprocal, and $c_r = \cos(\theta_0)$ and $c_s = -\cos(\theta_0 - 2\varphi)$ are slant factors.

The normalized diffraction efficiency as a function of incident angle deviation is shown in figure 7 [30, 31]. The full width at half maximum is as high as 3.22°, which is beneficial to align the slanted HPDLC grating in a setup. The special characteristic of the slanted HPDLC grating is that the Bragg diffraction is asymmetric with the deviation angle, as shown in figure 7. The distances from the maximum to the first minimum are 3.4° and −3.25°, respectively. The diffraction efficiency of the first side lobe is 1.85 times higher than that of the minus first side lobe. The coupled-wave theoretical fitting curve is also plotted in figure 7. The agreement between the experiment and the coupled-wave theory is acceptable. The discrepancy between the experiment and the coupled-wave theory for the first side lode is caused by the anisotropic characterization of the slanted HPDCL grating [32]. The refractive index modulation $\Delta n = 0.0224$ is determined by the Jones matrix method [33]. The transmittance spectrum as a function of wavelength for the slanted HPDLC is shown in figure 8. The Bragg gap centers at 615 nm, which is generated by the slanted HPDLC grating [34]. The transmittance of the slanted HPDLC grating increases with the sampling wavelength without the gap in the visible spectrum band.

3.4. Electrical field switching

Thanks to the positive nematic LC in the slanted HPDLC grating, the grating can be switched because of the reorientation of the LC with external electric field [35]. The normalized diffraction efficiency as a function of root mean square (RMS) driving electric field is shown in figure 9. The diffraction efficiency value decreases and reaches a constant with the driving electric field. The electric field for the diffraction efficiency drops to 90 and 10% to the initial value is 5.8 and 12.0 V μm^{-1}, respectively. The diffraction efficiency cannot reach zero because the refractive index of the polymer n_p is not equal to the ordinary refractive index n_o of the LC. The slanted HPDLC grating can be used to achieve polarized light beam steering modulation using the electric field induced switching property.

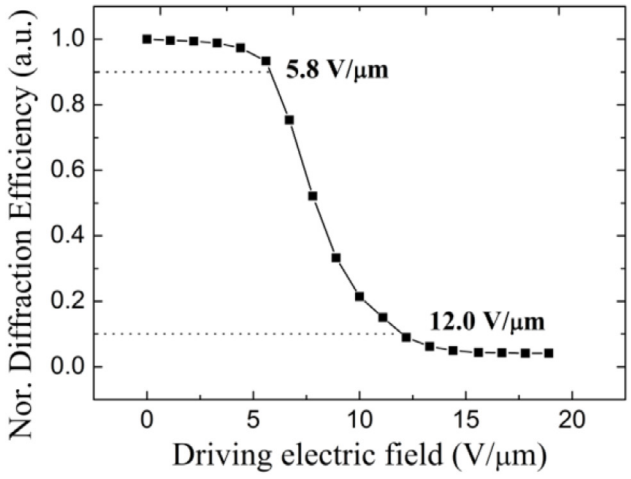

Figure 9. Electrically switching for the slanted HPDLC grating.

4. Conclusions

In summary, the 16.6° slanted HPDLC grating with diffraction efficiency up to 80% was fabricated using a holographic technique. The SEM image confirmed the slanted grating configuration. The grating showed anisotropic diffraction characteristics. The diffraction efficiency for the *p*-polarized light was as high as 80%. The 65° beam steering was implemented using the slanted HPDLC grating with a polarized He–Ne laser. The slanted HPDLC grating can be switched with external electric field. The results in this work provide an optional method to fabricate a slanted grating configuration. The slanted HPDLC grating can be used in the field where polarized beam steering is required.

Acknowledgments

This work was supported by the National Natural Science Foundation of China under Grant Nos. 11704378, 11604327, 61775212, 61377032 and 61378075.

Author contributions

Minghuan Liu and Zhihui Diao conceived and designed the experiments; Minghuan Liu and Zhihui Diao performed the experiments; Minghuan Liu, Quanquan Mu and Zhaoliang Cao analyzed the data; Yonggang Liu, Zenghui Peng, Lishuang Yao and Li Xuan contributed reagents/materials/analysis tools; Minghuan Liu wrote the paper. All authors have approved the final article.

Conflicts of interest

The authors declare no conflict of interest.

ORCID iDs

Minghuan Liu https://orcid.org/0000-0001-9341-1850

References

[1] Peng H *et al* 2014 *J. Am. Chem. Soc.* **136** 8855–8
[2] Peng H Y, Chen G N, Ni M L, Yan Y, Zhuang J Q, Roy V A L, Li R KY and Xie X L 2015 *Polym. Chem.* **6** 8259–69
[3] Bunning T J, Natarajan L V, Tondiglia V P and Sutherland R L 2000 *Annu. Rev. Mater. Sci.* **30** 83–115
[4] Malinauskas M, Zukauskas A, Hasegawa S, Hayasaki Y, Mizeikis V, Buividas R and Juodkazis S 2016 *Light Sci. Appl.* **5** e16133
[5] Bonefacino J, Tam H Y, Glen T S, Cheng X, Pun C F J, Wang J, Lee P H, Tse M L V and Boles S T 2018 *Light Sci. Appl.* **7** 17161
[6] Ogiwara A and Watanabe M 2012 *Appl. Opt.* **51** 5168–77
[7] Vasil'ev P P, Penty R V and White I H 2016 *Light Sci. Appl.* **5** e16086
[8] Papaioannou M, Plum E, Valente J, Rogers E T F and Zheludev N I 2016 *Light Sci. Appl.* **5** e16070
[9] Yang J *et al* 2016 *Light Sci. Appl.* **5** e16046
[10] Ding F, Deshpande R and Bozhevolnyi S I 2018 *Light Sci. Appl.* **7** 17178
[11] Ahmed R, Yetisen A K, Yun S H and Butt H 2017 *Light Sci. Appl.* **6** e16214
[12] Chen X *et al* 2017 *Light Sci. Appl.* **6** e16190
[13] Escuti M J, Kossyrev P, Crawford G P, Fiske T G, Colegrove J and Silverstein L D 2000 *Appl. Phys. Lett.* **77** 4262–4
[14] Xianyu H, Qi J, Cohn R F and Crawford G P 2003 *Opt. Lett.* **28** 792–4
[15] Yau S M, Kok M H and Tam W Y 2008 *J. Opt. A: Pure Appl. Opt.* **10** 015201
[16] Sun X H, Tao X M, Ye T J, Szeto Y S and Cheng X Y 2005 *J. Appl. Phys.* **98** 043510
[17] Kakiuchida H, Tazawa M, Yoshimura K and Ogiwara A 2010 *Sol. Energy Mater. Sol. Cells* **94** 1747–52
[18] Fernández R, Gallego S, Navarro-Fuster V, Neipp C, Francés J, Fenoll S, Pascual I and Beléndez A 2016 *Opt. Mater. Express* **6** 3455
[19] Neipp C, Francés J, Martínez F J, Fernández R, Alvarez M L, Bleda S, Ortuño M and Gallego S 2017 *Polymers* **9** 395
[20] Presnyakov V, Asatryan K, Galstian T and Chigrinov V 2006 *Opt. Express* **14** 10558–64
[21] Moothanchery M, Naydenova I and Toal V 2011 *Opt. Express* **19** 13395–404
[22] Liu M, Liu Y, Peng Z, Mu Q, Cao Z, Lu X, Ma J and Xuan L 2017 *J. Phys. D: Appl. Phys.* **50** 315103
[23] Liu M H, Liu Y G, Peng Z H, Zhao H F, Cao Z L and Xuan L 2017 *Appl. Phys.* B **123** 208
[24] Manaka T and Iwamoto M 2016 *Light Sci. Appl.* **5** e16040
[25] Ciattoni A, Marini A, Rizza C and Conti C 2018 *Light Sci. Appl.* **7** 5
[26] Huang W, Liu Y, Diao Z, Yang C, Yao L, Ma J and Xuan L 2012 *Appl. Opt.* **51** 4013–20
[27] Huang W B, Pu D L, Shen S, Wei G J, Xuan L and Chen L S 2015 *J. Phys. D: Appl. Phys.* **48** 375303
[28] Wang B, Jiang J and Nordin G P 2004 *Opt. Express* **12** 3313–26
[29] Kogelnik H 1969 *Bell Syst. Tech. J.* **48** 2909–47
[30] Li T, Cao L C, He Q S and Jin G F 2012 *Proc. SPIE* **8556** 85560O
[31] Vojtisek P, Kveton M and Richter I 2016 *Proc. SPIE* **10151** 1015115
[32] Montemezzani G and Zgonik M 1997 *Phys. Rev.* E **55** 1035–47
[33] Caputo R, Trebisacce I, De Sio L and Umeton C 2010 *Opt. Express* **18** 5776–84
[34] Kok M H, Ma R, Lee J C W, Tam W Y, Chan C T, Sheng P and Cheah K W 2005 *Phys. Rev.* E **72** 047601
[35] Liu Y J, Sun X W, Liu J H, Dai H T and Xu K S 2005 *Appl. Phys. Lett.* **86** 041115